An Improved Particle Filter With a Novel Hybrid Proposal Distribution for Quantitative Analysis of Gold Immunochromatographic Strips

Nianyin Zeng, Zidong Wang, *Fellow, IEEE*, Hong Zhang, Kee-Eung Kim, Yurong Li, and Xiaohui Liu

***Abstract*—In this paper, a novel statistical pattern recognition method is proposed for accurately segmenting test and control lines from the gold immunochromatographic strip (GICS) images for the benefits of quantitative analysis. A new dynamic state-space model is established, based on which the segmentation task of test and control lines is transformed into a state estimation problem. Especially, the transition equation is utilized to describe the relationship between contour points on the upper and the lower boundaries of test and control lines, and a new observation equation is developed by combining the contrast of between-class variance and the uniformity measure. Then, an innovative particle filter (PF) with a hybrid proposal distribution, namely, deep-belief-network-based particle filter (DBN-PF) is put forward, where the deep belief network (DBN) provides an initial recognition result in the hybrid proposal distribution, and the particle swarm optimization algorithm moves particles to regions of high likelihood. The performance of proposed DBN-PF method is comprehensively evaluated on not only an artificial dataset but also the GICS images in terms of several indices as compared to the PF and DBN methods. It is demonstrated via experiment results that the proposed approach is effective in quantitative analysis of GICS.**

***Index Terms*—Gold immunochromatographic strip, particle filter, proposal distribution, deep belief network, dynamical model, image segmentation, particle swarm optimization algorithm, Monte Carlo.**

Manuscript received June 18, 2019; accepted July 27, 2019. Date of publication August 6, 2019; date of current version August 13, 2019. This work was supported in part by the UK-China Industry Academia Partnership Programme under Grant UK-CIAPP-276, in part by the Korea Foundation for Advanced Studies, in part by the Natural Science Foundation of China under Grants 61873148, 61403319, and 61773124, in part by the International Science and Technology Cooperation Project of Fujian Province of China under Grant 2019I0003, in part by the Fundamental Research Funds for the Central Universities in China under Grant 20720190009, and in part by the Fujian Provincial Key Laboratory of Eco-Industrial Green Technology of China. The review of this paper was arranged by Associate Editor Huigao Duan. *(Corresponding author: Zidong Wang.)*

N. Zeng and H. Zhang are with the Department of Instrumental and Electrical Engineering, Xiamen University, Fujian 361005, China (e-mail: zny@xmu.edu.cn; zhanghong@stu.xmu.edu.cn).

Z. Wang and X. Liu are with the Department of Computer Science, Brunel University London, Uxbridge UB8 3PH, U.K. (e-mail: Zidong.Wang@brunel.ac.uk; Xiaohui.Liu@brunel.ac.uk).

K.-E. Kim is with the Department of Computer Science, Korea Advanced Institute of Science and Technology, Daejeon 305-701, South Korea (e-mail: keeeung.kim@kaist.edu).

Y. Li is with the College of Electrical Engineering and Automation, Fuzhou University, Fuzhou 350002, China, and also with the Fujian Key Laboratory of Medical Instrumentation and Pharmaceutical Technology, Fuzhou 350002, China (e-mail: liyurong@fzu.edu.cn).

Digital Object Identifier 10.1109/TNANO.2019.2932271

I. Introduction

NOWADAYS, biosensors have shown promising applications in various fields including global and public health care, environmental research, agriculture and forensic sciences. The gold immunochromatographic strip (GICS), as a kind of lateral flow immunoassay, provides a unique point-of-care (POC) test platform for the detection of various analytes with high sensitivity, good specificity and short turnaround time [26], [31], [37]. In particular, the GICS can achieve rapid detection of target analytes in samples via transforming them into more easily detectable signals on the test line by using nano-gold particles, see Fig. 1 for the schematic diagram of the GICS. Currently, the image-based quantitative test system, which can acquire the color intensity of nono-gold labeled complexes in the test line (signal intensity) has already shown promising application potentials of the advance image processing techniques.

In recent years, great efforts have been devoted to the widening of the range of GICS applications and also the enhancement of the detection performance of GICS by biochemistry researchers [15], [26], [31], [43], [44]. In addition, there is an increasing research interest in modeling the biochemical process of GICS so as to optimize the characteristics of GICS [2], [20], [23], [28], [41], [42]. In particular, we refer the readers to two recent reviews [6], [27], and the reference therein for more details. In fact, the practical need for more meaningful diagnostics with quantitative results has been the thruster of the development of image-based quantitative POC test systems that are capable of quantitatively detecting target analytes in samples. A focus of research along this direction has been on how to accurately extract the test and control lines from GICS images via image segmentation methods including the Otsu threshold segmentation algorithm, the fuzzy c-means (FCM) clustering approach, the cellular neural network (CNN) as well as some latest algorithms in machine learning such as the deep belief network (DBN) [4], [16], [19], [32], [39], [43].

It should be pointed out that it is indeed challenging to accurately segment the test and control lines from GICS images that exhibit inherent characteristics outlined as follows. First, the boundaries of test and control lines are usually neither clear nor definite (actually quite blurry) especially when the color of the test line is relatively shallow. Second, the boundaries of test and control lines are irregular yet serrated (i.e., not as smooth as they seem to be) since both lines are generally sprayed on

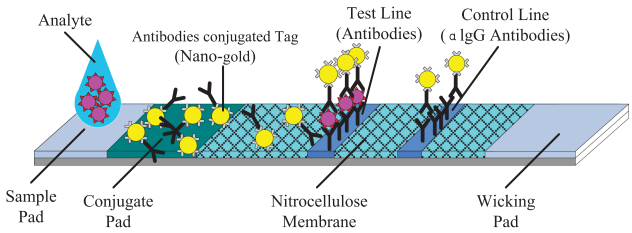

Fig. 1. Schematic diagram of the sandwich-type GICS.

the strip in a non-uniform manner. Furthermore, the reading window of GICS images inevitably contains some interference noises when the sample to be detected (e.g. urine, blood and serum) flows over the membrane. To overcome the challenges listed above, we attempt to establish a dynamic state-space model for the segmentation of control line and test line, where the state sequence represents the contour points of boundaries. Then, we intend to develop a particle filter (PF) architecture, in combination with the deep belief network (DBN) and the particle swarm optimization (PSO) algorithm, for quantitative interpretation of the GICS by accurately recognizing the test and control lines from the obtained GICS images.

As a sequential Monto Carlo technique, the PF has been proven to be capable of dealing with nonlinear and non-Gaussian problems [1], [42]. The greatest advantage of the PF method is its suitability of representing the posterior distribution of states by a set of random particles with associated weights. Over the last few decades, the research on PF algorithms has maintained a good momentum with remarkable progress in the application of target tracking, signal and information processing, automation and system modeling, etc [7], [10], [12], [13], [24], [29], [30], [38], [42]. It is worth noticing that the PF approach has been successfully applied to some image segmentation issues, see e.g. [3], [34], [36]. In particular, a deep particle filter was proposed in [3] for dynamically segmenting the left ventricle endocardium, in which deep learning architectures were employed as the observation distribution and the results of transition and observation models were combined to obtain the proposal distribution.

To investigate the segmentation of GICS images by the PF approach, it is often necessary to establish a dynamic state-space model [3] that consists of the transition and observation equations, based on which the segmentation problem can be transformed into an equivalent state estimation problem. In practice, however, it is rather difficult to acquire the observation and transition distributions of the corresponding model. In this paper, a transition model is proposed to describe the relationship between contour points on the upper and lower boundaries of test and control lines. Then, a new observation model is developed by a combination of two evaluation indices, which are the contrast of between-class variance (CBCV) and uniformity measure (UM). Based on the established model, the PF method would stand out as a competitive candidate to address the optimal solution to the state estimation problem.

For standard PF where the transition prior is exploited as the proposal distribution, there is a degeneracy problem since the latest available information cannot be utilized to generate new values for the states. Furthermore, such kind of standard PF might not work efficiently since only a few particles can survive after some iterations (i.e., most particles have negligible weight). In theory, the choice of proposal distribution is of vital importance to the performance of the PF method. In this paper, we aim to develop a novel proposal distribution that utilizes a combination of deep belief network (DBN) and particle swarm optimization (PSO) algorithm in order to improve the performance of the PF approach. DBN, originally proposed by Hinton, is a greedy and hierarchical learning model that has been extensively investigated and widely applied in the field of machine learning [9], [21], [22], [25], [35], [39]. For example, in our recent work [39] proposed, a DBN method has been exploited to extract test and control lines from GICS images with a remarkable segmentation performance. Nevertheless, if we were to generate a swarm consisting of particles with recognition results by DBN method, the computational burden might be unbearable with sacrificed diversity. In this case, as a global stochastic optimization algorithm, the PSO algorithm developed by Kennedy and Eberhart [11] is introduced in this paper to generate the swarm as well as move particles to regions of high likelihood.

The main contributions of this paper is primarily threefold. 1) A dynamic state-space model has been established for transforming the segmentation problem into the problem of state estimation. 2) The proposed dynamic state-space model consists of the transition equation which describes the relationship between contour points of the object to be segmented, and the observation equation which is formed by a combination of the contrast of between-class variance (CBCV) and uniformity measure (UM). 3) An innovative PF framework, which utilizes a combination of DBN and PSO algorithm as the proposal distribution, is proposed for segmenting the GICS images for the benefits of quantitative analysis.

The remainder of this paper is organized as follows. In Section II, the preliminaries about particle filter, deep belief network, as well as particle swarm optimization algorithm are presented. A dynamic state-space model for GICS images segmentation is established in Section III. Section IV provides a detailed introduction on the proposed DBN-PF segmentation framework. In Section V, the performance of the proposed DBN-PF approach is evaluated not only on an artificial dataset but also on the segmentation of GICS images. Finally, conclusions are drawn in Section VI.

II. Preliminaries

In this section, we first briefly describe the basic theory of particle filter (PF) methodology. Then, a brief and necessary subsection is provided to introduce the deep belief network (DBN) as well as its core component named Restricted Boltzmann Machine (RBM). In the end, the particle swarm optimization (PSO) algorithm is introduced to move particles to regions of high likelihood based on results of the trained DBN.

A. Particle Filter

Particle filter (PF) is a recursive Bayesian method based on the non-parametric Monte Carlo simulation [5], [33], [42]. Generally, PF is able to be applied to any nonlinear systems with an accuracy approximating to the optimum estimate.

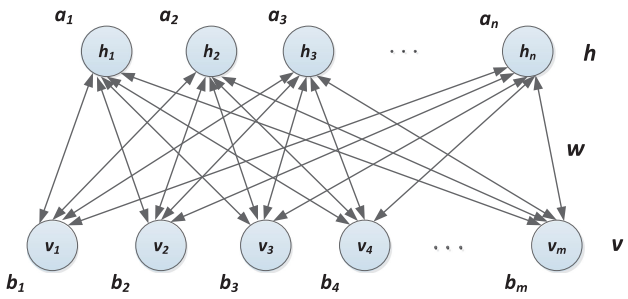

Fig. 2. Schematic diagram of RBM.

Consider the dynamic state space model of a nonlinear system as follows:

$$\text{State transition model:} \quad x_t = f(x_{t-1}, w_{t-1}) \tag{1}$$

$$\text{Observation model:} \quad y_t = g(x_t, v_t) \tag{2}$$

where t is the time index. x_t and y_t represent the state and observation variables, respectively. $f(\cdot)$ and $g(\cdot)$ represent the state transition and observation functions, respectively. w_t and v_t denote independently and identically distributed noises of process and measurement, respectively.

According to the law of large numbers, the PF is designed to approximate the posterior distribution $p(x_t|y_{1:t})$ via a set of weighted samples $\{x_t^i, w_t^i\}_{i=1}^N$, which are drawn from an importance proposal distribution $q(\cdot)$, i.e. $\{x_t^i \sim q(x_t|x_{t-1}^i, y_{1:t})\}$ $(i = 1, \ldots, N)$. The weight for each sample can be calculated by the following recursive formula:

$$w_t^i = w_{t-1}^i \frac{p(y_t|x_t^i)p(x_t^i|x_{t-1}^i)}{q(x_t|x_{t-1}^i, y_{1:t})} \tag{3}$$

Finally, the estimated state can be approximated by weighted sum of N samples:

$$\hat{x_t} \approx \sum_{i=1}^{N} \widetilde{w}_t^i x_t^i \tag{4}$$

where $\widetilde{w}_t^i$ is the normalized weight:

$$\widetilde{w}_t^i = w_t^i \frac{1}{\sum_{j=1}^N w_t^j} \tag{5}$$

B. Deep Belief Network

1) Restricted Boltzmann Machine: The Restricted Boltzmann Machine (RBM) is a stochastic neural network that can learn the distribution of input data [9], [39]. As shown in Fig. 2, the network also severs as a bipartite graph composed by one visible layer and one hidden layer, where visible units v are connected to hidden units h by a set of weighted connections. Especially, there are no connections existing between two units in the same layer.

The joint probability distribution $p(v, h|\theta)$ between visible and hidden layers in an RBM can be defined as follows:

$$p(v, h|\theta) = \frac{e^{-E(v,h|\theta)}}{Z(\theta)} \tag{6}$$

where $E(v, h|\theta) = -\sum_{i=1}^m \sum_{j=1}^n w_{ij} v_i h_j - \sum_{i=1}^m b_i v_i - \sum_{j=1}^n a_j h_j$ denotes the energy function, $Z(\theta) = \sum_{v,h} e^{-E(v,h|\theta)}$ denotes the partition function, and $\theta = (w, b, a)$ is the model parameter. Then, the most concerned marginal probability of visible layer, termed the likelihood function, can be calculated by:

$$p(v|\theta) = \frac{\sum_h e^{-E(v,h|\theta)}}{Z(\theta)} \tag{7}$$

In particular, the conditional probabilities $p(h|v, \theta)$ and $p(v|h, \theta)$ can be easily computed by the simple law of algebraic addition since any two units in the same layer are independent from each other. Here we set the sigmoid function $\sigma(x) = (1 + e^{-x})^{-1}$ as the activation function, and the equations are given as:

$$p(h_j = 1|v, \theta) = \sigma\left(\sum_{i=1}^{m} w_{ij} v_i + a_j\right) \tag{8}$$

$$p(v_i = 1|h, \theta) = \sigma\left(\sum_{j=1}^{n} w_{ij} h_j + b_i\right) \tag{9}$$

The training procedure of an RBM is aimed to configure a desirable parameter $\theta = (w, b, a)$ for the whole network. The judgment criterion of network property is whether it well fits the given training data, which can be achieved by maximizing the log likelihood function:

$$\theta^* = \arg\max_{\theta} \sum_{t=1}^{T} \ln p(v^{(t)}|\theta) \tag{10}$$

where T represents the number of the training set.

Although the gradient ascent algorithm can be applied to obtain the gradient equation of each model parameter according to the objective function, the Gibbs sampling was introduced in [8] to approximate the joint probability distribution $p(v, h|\theta)$. Furthermore, a fast learning algorithm, named the contrastive divergence (CD) [8], was proposed to speed up the sampling process. In particular, CD algorithm performs satisfactorily for model recognition even at $k = 1$, which can be represented by:

$$h^{(0)} \sim p(h|v^{(0)}), \quad v^{(1)} \sim p(v|h^{(0)}) \tag{11}$$

Therefore, the update rules for parameters $\theta = (w, b, a)$ are given as:

$$w^{t+1} = w^t + \epsilon(p(h|v^{(0)})[v^{(0)}]^T - p(h|v^{(1)})[v^{(1)}]^T) \tag{12}$$

$$b^{t+1} = b^t + \epsilon(v^{(0)} - v^{(1)}) \tag{13}$$

$$a^{t+1} = a^t + \epsilon(p(h|v^{(0)}) - p(h|v^{(1)})) \tag{14}$$

where ϵ represents the learning rate and t represents the time index.

2) Deep Belief Network: Deep belief network (DBN), proposed by Hinton [9] in 2006, has been widely studied and extensively applied to deal with a variety of deep learning tasks. The DBN is a deep neural network composed by a stack of RBMs together with a logistic regression, as shown in Fig. 3. It is actually a greedy and hierarchical learning model, in which a bottom-up learning strategy is adopted. More specifically, the

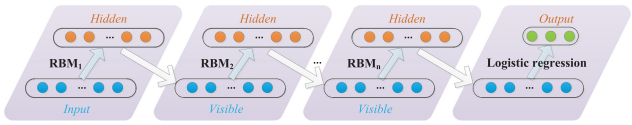

Fig. 3. Flowchart of DBN.

RBM at the bottom is firstly pre-trained using training data as its inputs. Once the parameters of the lower-layer RBM are determined, then the output of hidden feature activations can be utilized as the input of visible units for the higher-layer RBM. Finally, a logistic regression is added to the top of the stack of RBMs so that the network can achieve tasks such as classification, recognition and etc [39].

The training process of DBN includes two main phases: pre-training and fine-tuning. The pre-training stage is going to determine the unknown parameters of RBMs, i.e., $\theta = (w, b, a)$, with the CD algorithm mentioned above in a bottom-up manner. It is of essential importance for constructing a power configuration of DBN, which suffices desirable property of feature extraction. In the fine-tuning stage, a back propagation or gradient descent algorithm is used to make a slight adjustment of network parameters.

C. Particle Swarm Optimization Algorithm

Particle swarm optimization (PSO), proposed by Kennedy and Eberhart [11], is a global optimization algorithm illuminated by the wildlife population behaviors such as fish school or bird flock, etc. The basic PSO and improved PSOs have been extensively utilized to solve various practical issues, owing to its effectiveness of interpreting intractable optimization problem and its easy implementation with rapid convergence to a reasonable solution [14], [44], [45].

In PSO, particles of a swarm are aimed to find the global optimum, and they move with a certain velocity in iterations. During the procedure of optimization, each particle adjusts its velocity according to the optimal solution of individual and population. We suppose that a swarm including S particles flies in the D-dimensional search space. At tth iteration, the position and velocity of the ith particle are respectively expressed by $x_i(t) = (x_{i1}(t), x_{i2}(t), \ldots, x_{iD}(t))$ and $v_i(t) = (v_{i1}(t), v_{i2}(t), \ldots, v_{iD}(t))$. Similarly, the optimal solution of individual and population are denoted by $p_i(t) = (p_{i1}(t), p_{i2}(t), \ldots, p_{iD}(t))$ and $p_g(t) = (p_{g1}(t), p_{g2}(t), \ldots, p_{gD}(t))$, which represent the best position encountered by itself and the best position in the whole swarm, respectively. Then, the update equations of particles are described as follows:

$$\begin{aligned} v_{id}(t+1) &= w \times v_{id}(t) + c_1 \times r_1 \times (p_{id}(t) - x_{id}(t)) \\ &\quad + c_2 \times r_2 \times (p_{gd}(t) - x_{id}(t)), \\ x_{id}(t+1) &= x_{id}(t) + v_{id}(t+1), \end{aligned} \tag{15}$$

where w represents the inertia weight, c_1 and c_2 denote acceleration coefficients, r_1 and r_2 denote two random numbers from [0,1].

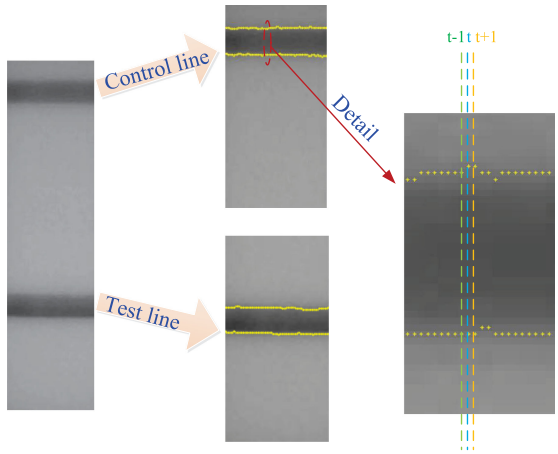

Fig. 4. The diagram of the GICS image segmentation based on the dynamic model. Left: The detection window of GICS image; Middle: Segmentation contour with yellow markers; Right: Detailed sequential annotation of the segmentation contour.

III. Dynamic State-Space Model for GICS Images Segmentation

Gold immunochromatographic strip (GICS), labeled with the colloidal gold nanoparticle, is an immunochromatographic methodology based on the high specificity of antigen-antibody interaction. Recently, image-based quantitative analysis of GICS has become a hotspot for research and there is a practical need to develop an effective image segmentation approach to accurately extract the test and control lines from GICS images. Generally, the GICS images acquired by the established quantitative instrument [39] should be preprocessed at first so as to obtain the detection window of GICS, as shown in Fig. 4. Therefore, the problem of segmenting test and control lines from GICS images can be transformed into that of determining the upper and lower boundaries contour points of test or control line, which can be represented by a state sequence denoted by $\{x_t | t \in T\}$, $x_t \in R^2$. In this context, the problem to be solved in this paper can be considered as the state estimation problem of a state-space model, where the transition distribution in the model is represented by $p(x_t|x_{t-1})$ and the observations $\{y_t|t \in T\}$ ($y_t \in R$) are conditionally independent given the process $\{x_t|t \in T\}$ with marginal distribution $p(y_t|x_t)$.

A. Transition Model

In order to segment the GICS images, a transition model should be developed so as to describe the relationship between contour points on the upper and lower boundaries of test and control lines. It should be mentioned that the upper and lower boundaries of test and control lines are irregular (not as smooth as they seem), which might be resulted from various external factors, such as temperature, humidity, colloidal gold and non-uniform permeation of specimens [43]. Here, we model the relationship between contour points by the following discrete-time dynamic system:

$$x_t = x_{t-1} + v_{t-1} \tag{16}$$

where v_{t-1} represents the system noise, which is typically determined by the structure, reaction rates, and concentrations of antibodies, antigens, or complex material [41]. It can be considered as the zero-mean uncorrelated Gaussian noises (with covariance $Q = 2$ in this paper) due to the random nature as well as the different sources for the system noise.

B. Observation Model

In this paper, a new observation model is developed by a combination of the contrast of between-class variance (CBCV) and uniformity measure (UM). Note that the CBCV and UM are widely used as evaluation indices for the performance of image segmentation [40].

For a gray-level image $f(m,n)$, we assume the state to be x_t at time t, and the corresponding CBCV can then be calculated by the following equations [40]:

$$CBCV(x_t) = w_0 \times w_1 \times (\mu_0 - \mu_1)^2 \tag{17}$$

where

$$w_0 = \frac{K_{x_t}}{K_0}, \quad w_1 = 1 - \frac{K_{x_t}}{K_0} \tag{18}$$

$$\mu_0 = \frac{1}{K_{x_t}} \sum_{(m,n)\in R_{x_t}} f(m,n), \quad \mu_1 = \frac{1}{K_0} \sum_{(m,n)\in R_0} f(m,n) \tag{19}$$

Here, R_{x_t} and R_0 represent the areas of segmentation region and the whole detection region, K_{x_t} and K_0 represent the pixel numbers of segmentation region and the whole detection region, respectively. Therefore, w_0 and w_1 denote the proportions of segmentation region and background. μ_0 and μ_1 denote the average gray-values of segmentation region and background.

The UM is defined as the similarity of property about region element, which can be calculated based on the variance of the feature evaluated at each pixel belonging to the region [40]. Therefore, for a gray-level image $f(m,n)$, the UM at time t can be computed as follows:

$$UM(x_t) = 1\frac{1}{\beta}\left\{ \sum_{(m,n)\in R_{x_t}} \left[f(m,n) - \frac{1}{K_{x_t}} \sum_{(m,n)\in R_{x_t}} f(m,n) \right]^2 \right\} \tag{20}$$

where β is a normalization factor. Therefore, the observation model for GICS images can be modeled as:

$$f(x_t) = \alpha CBCV(x_t) + \gamma UM(x_t) + m_t \tag{21}$$

where α and γ are the weighting coefficients, m_t stands for the measurement noise. Meanwhile, the corresponding observation distribution $p(y_t|x_t)$ can be described as the following likelihood distribution:

$$p(y_t|x_t) \propto e^{\frac{1}{f(x_t)}} \tag{22}$$

IV. DBN-PF Method for Segmenting GICS Images

The main task that we like to accomplish in this study is the delineation of upper and lower boundaries contour points of test and control lines, namely, the state sequence $\{x_t | t \in T\}$. In general, the optimal solution to the state estimation problem can be obtained by the PF approach based on the previously established dynamic state-space model. However, the standard PF (where the transition prior is employed as the proposal distribution) has a degeneracy problem since it ignores the most recent evidence y_t and therefore only a few particles can survive. In this case, it is of vital importance to choose an efficient proposal distribution in the particle filter method. In particular, various intelligent methods have been proposed to optimize the distribution of particles in their propagation process in the PF, which can be find in the survey paper [17]. For this purpose, an innovative particle filter framework, namely, deep-belief-network-based particle filter (DBN-PF), is proposed in this paper that utilizes a combination of DBN and PSO algorithm as the proposal distribution, see Fig. 5 for more details.

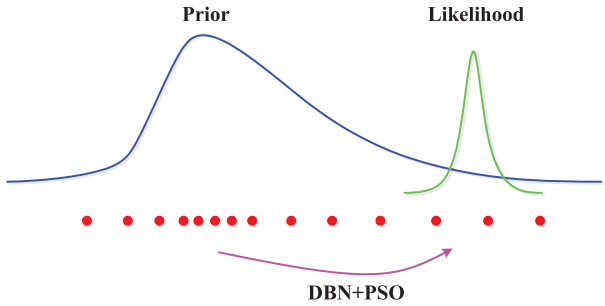

Fig. 5. The proposal distribution of the DBN-PF method.

To illustrate proposed DBN-PF method, the role of DBN is to first provide an initial recognition result. According to the characteristic of GICS images, three features (namely, the gray intensity, distance and difference features) are selected as the input of the DBN so as to distinguish the control and test lines. For each pixel in the region of interest, a square window $winsize \times winsize$ in the neighborhood are extracted to obtain gray intensity of pixels. Note that, for pixels near the image border, a mirroring approach is introduced to get intensity values of regions inside the window but beyond the image border. In addition, the distance feature denotes the distance to the center and the difference feature stands for the difference of intensity values between two lines and background. Therefore, a discriminative DBN model, as shown in Fig. 6, is established to obtain the initial segmentation result based on the theory introduced in Section II-B.

Next, the PSO algorithm is utilized to move particles to regions of high likelihood. In particular, the observation model (21) is selected as the objective function of PSO. That is, the bigger the value of (21) the higher the likelihood. Compared with the transition prior, the proposal distribution of DBN-PF method takes advantage of the latest available information to generate new values for the states.

Remark 1: The weight w_t of DBN-PF method is upper bounded and, therefore, the convergence is ensured based on the theorem introduced in [33].

Remark 2: It is not always beneficial for PF to use the likelihood/observation information to adjust the prior. The method

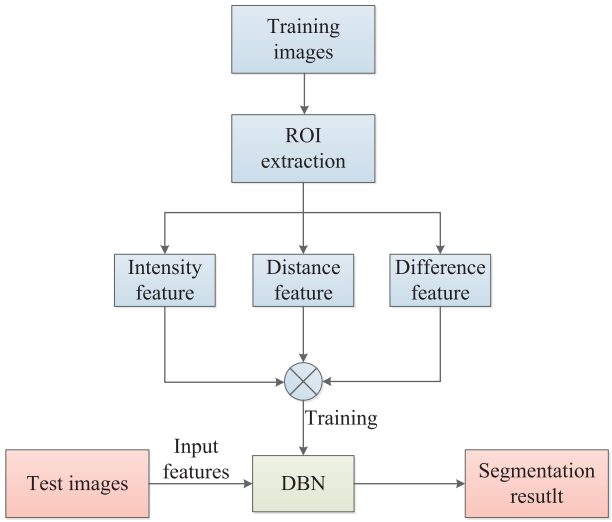

Fig. 6. Flow diagram of the DBN-based GICS image segmentation.

works well when the observation noise is comparably small, see the detailed analysis given in [18].

For a better illustration, the pseudocode of the proposed DBN-PF algorithm in this paper is described as follows:

(a) **Deep belief network**
  Calculate three discriminative features as the input of DBN X.
  Establish the DBN model and train the deep architecture $\theta = (w, b, a)$.
  Obtain the initial recognition result Y.
(b) **Particle swarm optimization algorithm**
  For $i = 1, 2, \ldots, N$
  Initialize the particles with acquired Y.
  Iterate the velocity and position of particles with the objective function (21)
  Update the individual-best p_i and global-best p_g.
(c) **For** $i = 1, 2, \ldots, N$**, sample** $\{x_t^i \sim q(x_t|x_{t-1}^i, y_{1:t})\}$ **according to PSO results**
(d) **For** $i = 1, 2, \ldots, N$**, evaluate the importance weights:**

$$w_t^i = w_{t-1}^i \frac{p(y_t|x_t^i)p(x_t^i|x_{t-1}^i)}{q(x_t|x_{t-1}^i, y_{1:t})}$$

(e) **For** $i = 1, 2, \ldots, N$**, normalize the weights:** $\widetilde{w}_t^i = w_t^i \frac{1}{\sum_{j=1}^N w_t^j}$
(f) **Resample procedure**
(g) **Output the estimated state:** $\hat{x}_t \approx \sum_{i=1}^N \widetilde{w}_t^i x_t^i$

V. Experimental Results and Discussions

In this section, a series of simulations and experimental tests are designed to show the effective of the proposed DBN-PF approach. To make the study more comprehensive and convincing, an artificial dataset is created in this paper on the basic of the characteristic of GICS images. In particular, the accuracy of image segmentation can be verified via the designed artificial dataset. After that, the proposed DBN-PF approach is utilized to solve the problem of GICS image segmentation. Furthermore, the performance of the proposed DBN-PF approach is also compared with those of PF and DBN in term of several indexes so as to demonstrate the superiority of the proposed algorithm.

In this paper, a four-layer DBN with 100 hidden nodes is established to accomplish the recognition task. The window size is set as 13 and the network has 171 input nodes. In the training procedure, the learning rate is set as 1, and the deep learning architecture iterates 20 times independently to reduce random effects in the experiments. In PSO, a swarm with 100 particles is generated to find out regions of high likelihood, the inertia weight w is set as 1.5 and the acceleration coefficients c_1 and c_2 are equal to 2. Note that two parameters α and γ in the observation model (21) are set as 0.5 and 1000, respectively.

A. Simulations on An Artificial Dataset

According to the characteristic of GICS images, an artificial image dataset composed by four groups is designed to accurately evaluate the performance of image segmentation, where each group includes eight images with different level of gray value. Especially, the line in each image which is similar to the test or control line in GICS images, has a serrated and blurry boundary. Besides, the dataset is disturbed by noises with different intensities. Therefore, it should be mentioned that these characteristics greatly increasing the difficulty for segmentation. Three trials are carried out when the number of blurry row n is set as 2, 3 and 4, respectively. Here, one of the groups in the dataset is shown in Fig. 7 ($n = 4$). In our experiments, three groups are used as the training set, and the remaining one is exploited as the testing set. Besides, a cross-validation method is utilized in this paper to guarantee the effectiveness of experiments, and the mean results are reported.

Here, we choose some representative cases to demonstrate the segmentation performance of different approaches. As shown in Fig. 8, the segmentation results are obtained when the group ($k = 4$, $n = 3$) corrupted by the largest additional white noise with standard deviation 2 is used as the testing data, while images 2, 8 represent different levels of gray value in Fig. 7.

Fig. 8 shows that there is a great difference in the segmentation performance among three methods. The traditional PF method yields the worst results among three methods, for the reason that there is a degradation problem when moving particles according to the state equation. The DBN method can achieve a relatively satisfactory result owing to its powerful learning capacity of deep architecture. However, it fails to recognize the serrated and blurry boundary of each image. It is worth pointing out it is the key and difficult to accurately segment the serrated and blurry boundary since it contains medical testing information in GICS images. In contrast, the proposed DBN-PF methodology obtains the best result, which can well distinguish the serrated and blurry boundaries.

Next, we calculate the accuracy of image segmentation by counting the proportion of pixels that are classified correctly. The segmentation accuracies are shown in Table I when the numbers of blurry row n equal to 2, 3 and 4, respectively.

It can be observed that the PF method obtains the lowest accuracy, which is lower than other two methods over 10%.

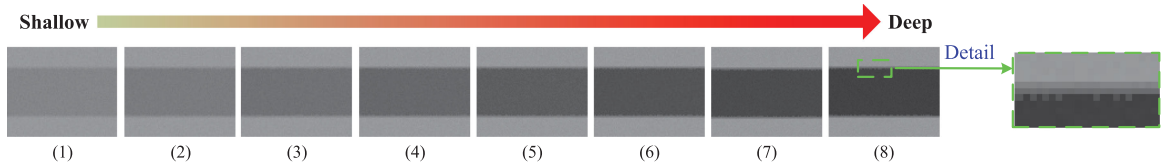

Fig. 7. One group of the artificial dataset includes eight images with different levels of gray value. The rightmost image is the detailed annotation of the serrated and blurry boundary ($n = 4$).

TABLE I
THE SEGMENTATION ACCURACY

Images	n=2			n=3			n=4		
	PF (%)	DBN (%)	DBN-PF (%)	PF (%)	DBN (%)	DBN-PF (%)	PF (%)	DBN (%)	DBN-PF (%)
1	86.623	98.846	99.670	88.071	98.846	99.509	88.278	98.642	99.046
2	86.318	98.765	99.617	87.954	98.562	99.657	88.525	98.765	99.238
3	87.488	98.765	99.701	88.250	98.444	99.664	88.540	98.772	99.037
4	86.537	98.765	99.698	86.864	98.463	99.664	88.852	98.917	99.16
5	87.154	98.765	99.701	87.494	98.488	99.704	89.586	98.920	99.040
6	86.454	98.765	99.694	86.889	98.469	99.651	88.034	99.000	99.037
7	86.309	98.765	99.682	87.775	98.491	99.719	88.855	98.959	99.043
8	87.537	98.756	99.664	86.667	98.488	99.667	88.429	98.843	98.973
Average	86.803	98.774	99.678	87.496	98.531	99.654	88.637	98.852	99.072

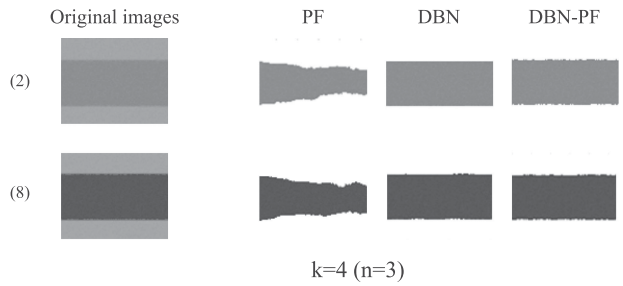

Fig. 8. Two typical simulation results of three approaches on the artificial dataset. Left column: Original images; Right column: Segmentation results of the PF, DBN and the proposed DBN-PF approaches.

Both DBN and proposed DBN-PF methods can provide high accuracy, while the proposed DBN-PF method outperforms the DBN method about 1%. There is an interesting phenomenon that the segmentation accuracy of the proposed DBN-PF method drops slightly when the number of blurry row is set as a bigger value ($n = 4$), while the DBN method remains steady. Nonetheless, the proposed DBN-PF method still outperforms the DBN method. The improvement of the proposed DBN-PF method may owe to the improved proposal distribution, which can move particles to regions of high likelihood. To verify this issue in more detail, therefore, the estimated filtering distributions by the PF and proposed DBN-PF approaches are shown in the Fig. 9.

From the Fig. 9, it is obvious that the posterior distributions obtained by the proposed DBN-PF approach are much more accurate than the posterior distributions obtained by the PF approach. The maximum probability of the posterior distributions obtained by the PF approach is 0.15, while the value obtained by the proposed DBN-PF approach is 0.5. Hence, the proposal distribution of the proposed DBN-PF approach is effective via considering the new observing information. The proposed DBN-PF approach can well solve the degeneracy problem of particle filters, therefore, it can provide an accurate estimation.

In addition, the value of objective function (21) for each image can be obtained and utilized to further verify the performance of DBN-PF method. The greater the value, the better the performance of the algorithm. The results are shown in Fig. 10 in the form of boxplot when the numbers of blurry row n equal to 2, 3 and 4, respectively. For the sake of simplicity, we only select 2 images from each test group which are (2) and (8) in Fig. 7 to show their values of objective function.

As shown in Fig. 10, the PF method provides not only the lowest mean values of the objection function but also more dispersive results. The DBN method can obtain a better performance, but is still lower than the proposed DBN-PF method. Compared to the other two methods, the proposed DBN-PF method yields superior results in most cases. Meanwhile, it is obviously that the proposed DBN-PF method provides a significant improvement over the traditional PF approach in the segmentation performance owing to the novel hybrid proposal distribution.

Finally, the impact of the number of particles for the proposed DBN-PF method is considered in this paper. The results of this part are depicted in Fig. 11.

From Fig. 11, we can find that the segmentation accuracy of the proposed DBN-PF approach is increasing with the number of particles. In addition, the accuracy increases slightly when the number of particles over 100, while the computational complexity of the algorithm increases greatly. In order to balance the computational complexity and the accuracy of the algorithm, therefore, the number of particles is selected as 100 in this paper.

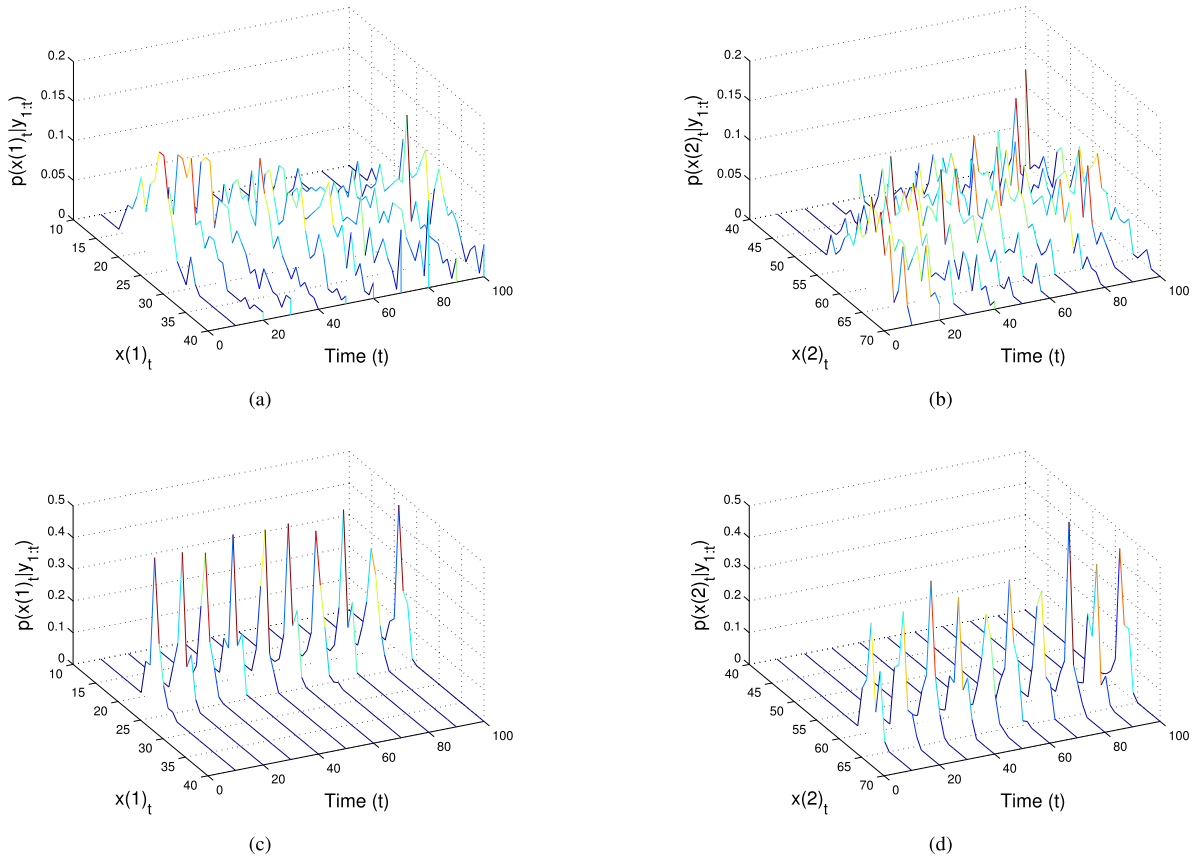

Fig. 9. Estimated filtering distributions by the PF and proposed DBN-PF approaches. (a) and (b): Posterior distributions of two dimensions of state via the PF approach. (c) and (d): Posterior distributions of two dimensions of state via the DBN-PF approach.

B. Simulations on GICS Images

1) Results of GICS Images Segmentation: In this section, we apply the proposed DBN-PF approach to the segmentation of GICS images. The objective is to extract the control line and test line which contain the useful information from GICS images. In our experiments, the human chorionic gonadotropin (hCG) is chosen as the analyte specimen. In particular, several groups of GICS images with different levels of specimen concentration from low to high are analyzed to demonstrate the performance of methods. Note that the color of test line is relative to the concentration of the analyte specimen. It should be pointed out that it is a challenging issue to accurately extract the test and control lines. For reasons of space and simplicity, two typical examples are utilized to demonstrate the segmentation performances, as shown in Fig. 12. Especially, the specimen concentrations are respectively set as 75 ml and 500 ml, representing the low and high concentrations.

From Fig. 12, it can be observed that all three approaches are capable to extract the control and test lines from the GICS images, even when the specimen concentration is at a low level. The extracted test and control lines obtained by the PF approach and the proposed DBN-PF approach are closer to the actual width of both lines than the result of DBN approach. That is, the results obtained by the DBN method are only part of the actual test and control lines. However, the boundary of test and control lines cannot be accurately recognized by the PF approach. In contrast, the proposed DBN-PF approach provides a satisfactory performance, which includes more effective information with a more accurate boundary. In addition, the value of objective function (21) for each GICS image is also utilized to further verify the performance of the proposed method. For the sake of simplicity, we similarly only select two typical results of three approaches for segmenting GICS images are shown in Fig. 13, and the corresponding concentrations are 75 ml and 500 ml, respectively.

As shown in Fig. 13, the proposed DBN-PF approach can obtain the biggest mean value of objective function among three methods both in the control line and test line, and also the mean square errors of the DBN-PF method are relatively minimum in most cases. Hence, the DBN-PF method outperforms the other two approaches.

2) Quantitative Analysis of the GICS: In order to achieve the quantitative determination of analyte specimen, a feature parameter, termed relative integral optical density ($RIOD$) is introduced to characterize the result of GICS. It is defined by the ratio of integral optical density (IOD) of the control line and test line, which is described by the following equation [43]:

$$RIOD = \frac{IOD_t}{IOD_c} = \frac{\sum_{i=1}^{N} \lg \frac{G_0}{G_t{}^i}}{\sum_{j=1}^{M} \lg \frac{G_0}{G_c{}^j}} \tag{23}$$

where IOD_t and IOD_c represent values of IOD for the test line and control line, and G_t and G_c denote the gray intensity of

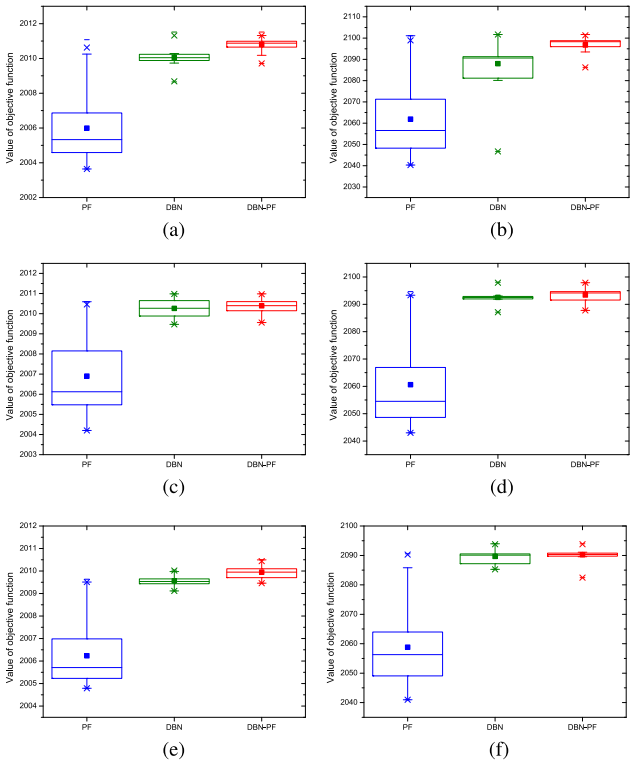

Fig. 10. Simulation results of three approaches on the artificial dataset. (a–b): The value of objective function when n is set as 2. (c–d): The value of objective function when n is set as 3. (e–f): The value of objective function when n is set as 4.

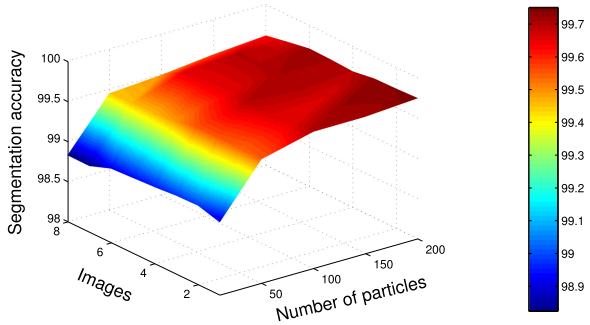

Fig. 11. The impact of the number of particles on the segmentation accuracy.

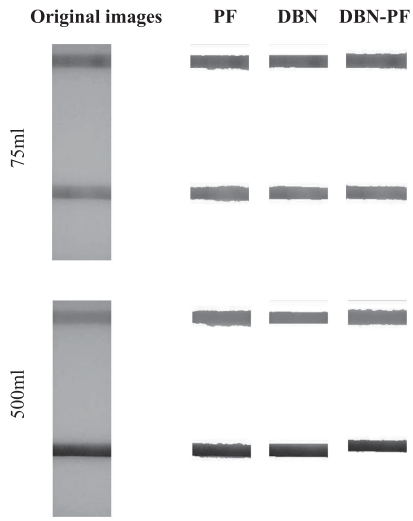

Fig. 12. Simulation results of three approaches for segmenting the GICS images. Left column: Original images with different levels of specimen concentration; Right column: Segmentation results of the PF, DBN and the proposed DBN-PF approaches.

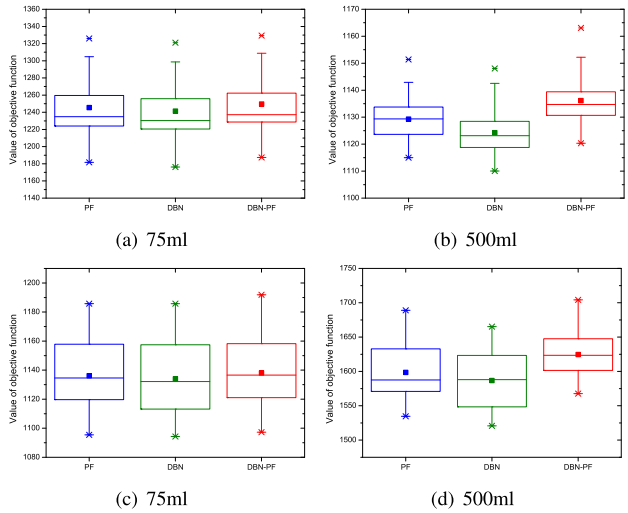

Fig. 13. Two typical simulation results of three approaches for segmenting the GICS images. (a–b): The value of objective function on the control line. (c–d): The value of objective function on the test line.

pixels on the test and control lines, respectively. G_0 stands for the mean value of gray intensity in the reading window. After that, the least square approach is applied to get straight fitted lines for four methods, as shown in Fig. 14, on the basis of the $RIOD$ points acquired by the segmentation results of GICS images under different concentrations.

For a comprehensive comparison, we compare the results of proposed DBN-PF method with traditional PF, DBN and the SDPSO-based CNN method developed in [43]. As shown in Fig. 14, all four approaches present a good corresponding relationship between the hCG concentration and the value of $RIOD$. That is, the $RIOD$ is suitable for being the feature parameter of GICS to realize the quantitative determination. For the same batch of quantitative strips, the fitted line is the working line when applied in the quantitative analysis of GICS. The bigger the correlation coefficient is, therefore, the more accurate the test result is. Hence, a detailed comparison among four methods has been made in Table II, where the correlation coefficient serves as an evaluation indicator.

From Table II, it can be inferred that the correlation coefficient of proposed DBN-PF approach is 0.982, while the PF approach and DBN approach are both 0.977, the SDPSO-based CNN method is 0.972. Therefore, the proposed DBN-PF approach is more suitable as a novel way of image-based method for quantitative analysis of GICS systems.

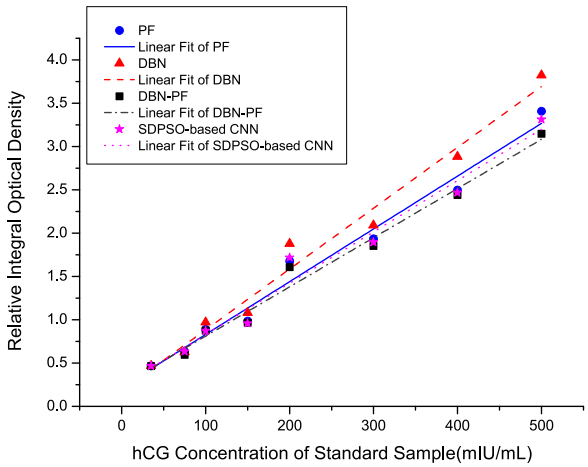

Fig. 14. Straight fitted lines for four methods based on the $RIOD$ points.

TABLE II
THE COMPARISON OF FITTING RESULTS AMONG FOUR METHODS

Method	Fitted linear equation	Correlation coefficient (%)
SDPSO-based CNN	y=0.006x+0.236	0.972
PF	y=0.006x+0.220	0.977
DBN	y=0.007x+0.182	0.977
DBN-PF	y=0.006x+0.244	0.982

VI. CONCLUSIONS

In this paper, a dynamic state-space model consisting of the transition and observation equations has been established, thereby facilitating the transforming of the image segmentation problem into the associated state estimation problem. Specifically, the transition equation describes the relationship between contour points on the upper and lower boundaries of test and control lines, and the observation equation is developed by a combination of the CBCV and UM. Meanwhile, we have developed an innovative PF, which utilizes a combination of DBN and PSO algorithm as the proposal distribution, to solve the problem of image segmentation and achieve the goal of quantitative analysis of GICS. Experimental results have demonstrated that the proposed DBN-PF approach can achieve superior performance when applied to the segmentation of GICS images. In particular, the proposed method can be considered as a new pattern recognition approach for the problem of image segmentation since simulation results have shown a significant improvement in the segmentation problem in terms of several indices. In the near future, some intelligent approaches [17] can be further investigated to fight sample degeneracy and impoverishment in the particle filters.

REFERENCES

[1] M. Arulampalam, S. Maskell, N. Gordon, and T. Clapp, "A tutorial on particle filters for online nonlinear/non-Gaussian Bayesian tracking," *IEEE Trans. Signal Process.*, vol. 50, no. 2, pp. 174–188, Feb. 2002.

[2] C. Berli and P. Kler, "A quantitative model for lateral flow assays," *Microfluidics Nanofluidics*, vol. 20, no. 7, 2016, Art. no. 104.

[3] G. Carneiro and J. Nascimento, "Combining multiple dynamic models and deep learning architectures for tracking the left ventricle endocardium in ultrasound data," *IEEE Trans. Pattern Anal. Mach. Intell.*, vol. 35, no. 11, pp. 2592–2607, Nov. 2013.

[4] L. Chuang, J. Hwang, H. Chang, F. Chang, and S. H. Jong, "Rapid and simple quantitative measurement of α-fetoprotein by combining immunochromatographic strip test and artificial neural network image analysis system," *Clinica Chimica Acta.*, vol. 348, pp. 87–93, 2004.

[5] A. Doucet, S. Godsill, and C. Andrieu, "On sequential Monte Carlo sampling methods for Bayesian filtering," *Statist. Comput.*, vol. 10, no. 3, pp. 197–208, 2000.

[6] D. Gasperino, T. Baughman, H. Hsieh, D. Bell, and B. Weigl, "Improving lateral flow assay performance using computational modeling," *Annu. Rev. Analytical Chem.*, vol. 11, pp. 219–244, 2018.

[7] W. Hu, J. Gao, J. Xing, C. Zhang, and S. Maybank, "Semi-supervised tensor-based graph embedding learning and its application to visual discriminant tracking," *IEEE Trans. Pattern Anal. Mach. Intell.*, vol. 39, no. 1, pp. 172–188, Jan. 2017.

[8] G. Hinton, S. Osindero, and Y. Teh, "A fast learning algorithm for deep belief nets," *Neural Comput.*, vol. 18, no. 7, pp. 1527–1554, 2006.

[9] G. Hinton and R. Salakhutdinov, "Reducing the dimensionality of data with neural networks," *Science*, vol. 313, no. 5786, pp. 504–507, 2006.

[10] S. Hiremath, G. Heijden, F. Evert, A. Stein, and C. Braak, "Laser range finder model for autonomous navigation of a robot in a maize field using a particle filter," *Comput. Electron. Agriculture*, vol. 100, pp. 41–50, 2014.

[11] J. Kennedy, "Particle swarm optimization," *Encyclopedia of Machine Learning*. Berlin, Germany: Springer, 2011, pp. 760–766.

[12] J. Kwon, H. Lee, F. Park, and K. Lee, "A geometric particle filter for template-based visual tracking," *IEEE Trans. Pattern Anal. Mach. Intell.*, vol. 36, no. 4, pp. 625–643, Apr. 2014.

[13] T. Li , M. Bolic, and P. Djuric, "Resampling methods for particle filtering: Classification, implementation, and strategies," *IEEE Signal Process. Mag.*, vol. 32, no. 3, pp. 70–86, May 2015.

[14] H. Li, T. Shen, and X. Huang, "Approximately global optimization for robust alignment of generalized shapes," *IEEE Trans. Pattern Anal. Mach. Intell.*, vol. 33, no. 6, pp. 1116–1131, Jun. 2011.

[15] J. Li, A. Ouellette, L. Giovangrandi, D. Cooper, A. Ricco, and G. Kovacs, "Optical scanner for immunoassays with up-converting phosphorescent labels," *IEEE Trans. Biomed. Eng.*, vol. 55, no. 5, pp. 1560–1571, May 2008.

[16] Y. Li, N. Zeng, and M. Du, "A novel image methodology for interpretation of gold immunochromatographic strip," *J. Comput.*, vol. 6, no. 3, pp. 540–547, 2011.

[17] T. Li, S. Sun, T. Sattar, and J. Corchado, "Fight sample degeneracy and impoverishment in particle filters: A review of intelligent approaches," *Expert Syst. Appl.*, vol. 41, no. 8, pp. 3944–3954, 2014.

[18] T. Li, J. Corchadoa, J. Bajo, S. Sun, and J. De Paz, "Effectiveness of Bayesian filters: An information fusion perspective," *Inf. Sci.*, vol. 329, pp. 670–689, 2016.

[19] C. Lin, C. Wu, H. Hsu, K. Li, and L. Lin, "Rapid bio-test strips reader with image processing technology," *Optik*, vol. 115, no. 8, pp. 363–369, 2004.

[20] Z. Liu, J. Hu, A. Li, S. Feng, Z. Qu, and F. Xu, "The effect of report particle properties on lateral flow assays: A mathematical model," *Sensors Actuators B, Chem.*, vol. 248, pp. 699–707, 2017.

[21] W. Liu, Z. Wang, X. Liu, N. Zeng, Y. Liu, and F. Alsaadi, "A survey of deep neural network architectures and their applications," *Neurocomputing*, vol. 234, pp. 11–26, 2017.

[22] A. Mohamed, G. Dahl, and G. Hinton, "Acoustic modeling using deep belief networks," *IEEE Trans. Audio, Speech, Lang. Process.*, vol. 20, no. 1, pp. 14–22, Jan. 2012.

[23] S. Qian and H. Haim, "A mathematical model of lateral flow bioreactions applied to sandwich assays," *Analytical Biochem.*, vol. 322, no. 1, pp. 89–98, 2003.

[24] J. Read, K. Achutegui, and J. Miguez, "A distributed particle filter for nonlinear tracking in wireless sensor networks," *Signal Process.*, vol. 98, pp. 121–134, 2014.

[25] M. Ranzato, V. Mnih, J. Susskind, and G. Hinton, "Modeling natural images using gated MRFs," *IEEE Trans. Pattern Anal. Mach. Intell.*, vol. 35, no. 9, pp. 2206–2222, Sep. 2013.

[26] C. Raphael and Y. Harley, *Lateral Flow Immunoassay*. Totowa, NJ, USA: Humana Press, 2008.

[27] D. V. Sotnikov, A. V. Zherdev, and B. B. Dzantiev, "Mathematical modeling of bioassays," *Biochem. Moscow*, vol. 28, no. 13, pp. 1744–1766, 2017.

[28] D. Sotnikov, A. Zherdev, and B. Dzantiev, "Mathematical model of serodiagnostic immunochromatographic assay," *Analytical Chem.*, vol. 89, no. 8, pp. 4419–4427, 2017.

[29] M. Sigalas, M. Pateraki, and P. Trahanias, "Full-body pose tracking—The top view reprojection approach," *IEEE Trans. Pattern Anal. Mach. Intell.*, vol. 38, no. 8, pp. 1569–1582, Aug. 2016.
[30] G. Shabat, Y. Shmueli, A. Bermanis, and A. Averbuch, "Accelerating particle filter using randomized multiscale and fast multipole type methods," *IEEE Trans. Pattern Anal. Mach. Intell.*, vol. 37, no. 7, pp. 1396–1407, Jul. 2015.
[31] M. Sajid, A. Kawde, and M. Daud, "Designs, formats and applications of lateral flow assay: A literature review," *J. Saudi Chem. Soc.*, vol. 19, no. 6, pp. 689–705, 2015.
[32] E. Sumonphan, S. Auephanwiriyakul, and N. Theera-Umpon, "Interpretation of nevirapine concentration from immunochromatographic strip test using support vector regression," in *Proc. IEEE Int. Conf. Mechatronics Autom.*, 200, pp. 633–637.
[33] R. Van Der Merwe, A. Doucet, N. De Freitas, and E. Wan, "The unscented particle filter," *in Proc. 13th Int. Conf. Neural Inf. Process. Syst.*, 2000, vol. 2000, pp. 584–590.
[34] D. Varas and F. Marques, "Region-based particle filter for video object segmentation," in *Proc. IEEE Conf. Comput. Vis. Pattern Recognit.*, 2014, pp. 3470–3477.
[35] D. Wu *et al.*, "Deep dynamic neural networks for multimodal gesture segmentation and recognition," *IEEE Trans. Pattern Anal. Mach. Intell.*, vol. 38, no. 8, pp. 1583–1597, Aug. 2016.
[36] N. Widynski and M. Mignotte, "A multiscale particle filter framework for contour detection," *IEEE Trans. Pattern Anal. Mach. Intell.*, vol. 36, no. 10, pp. 1922–1935, Oct. 2014.
[37] P. Yager *et al.*, "Microfuidic diagnostic technologies for global public health," *Nature* vol. 442, pp. 412–418, 2006.
[38] S. Yin and X. Zhu, "Intelligent particle filter and its application to fault detection of nonlinear system," *IEEE Trans. Ind. Electron.*, vol. 62, no. 6, pp. 3852–3861, Jun. 2015.
[39] N. Zeng, Z. Wang, H. Zhang, W. Liu, and F. Alsaadi, "Deep belief networks for quantitative analysis of a gold immunochromatographic strip," *Cogn. Comput.*, vol. 8, no. 4, pp. 684–692, 2016.
[40] Y. Zhang, "A survey on evaluation methods for image segmentation," *Pattern Recognit.*," vol. 29, no. 8, pp. 1335–1346, 1996.
[41] N. Zeng, Z. Wang, Y. Li, M. Du, and X. Liu, "A hybrid EKF and switching PSO algorithm for joint state and parameter estimation of lateral flow immunoassay models," *IEEE/ACM Trans. Comput. Biol. Bioinf.*, vol. 9, no. 2, pp. 321–329, Mar./Apr. 2012.
[42] N. Zeng, Z. Wang, Y. Li, M. Du, and X. Liu, "Identification of nonlinear lateral flow immunoassay state-space models via particle filter approach," *IEEE Trans. Nanotechnol.*, vol. 11, no. 2, pp. 321–327, Mar. 2012.
[43] N. Zeng *et al.*, "Image-based quantitative analysis of gold immunochromatographic strip via cellular neural network approach," *IEEE Trans. Med. Imag.*, vol. 33, no. 5, pp. 1129–1136, May 2014.
[44] N. Zeng, Z. Wang, H. Zhang, and F. E. Alsaadi, "A novel switching delayed PSO algorithm for estimating unknown parameters of lateral flow immunoassay," *Cogn. Comput.*, vol. 8, no. 2, pp. 143–152, 2016.
[45] N. Zeng, H. Zhang, W. Liu, J. Liang, and F. E. Alsaadi, "A switching delayed PSO optimized extreme learning machine for short-term load forecasting," *Neurocomputing*, vol. 240, pp. 175–182, 2017.

Nianyin Zeng was born in Fujian Province, China, in 1986. He received the B.Eng. degree in electrical engineering and automation and the Ph. D. degree in electrical engineering both from Fuzhou University, Fuzhou, China, in 2008 and 2013, respectively. From October 2012 to March 2013, he was a RA with the Department of Electrical and Electronic Engineering, the University of Hong Kong. From September 2017 to August 2018, he was an ISEF Fellow founded by the Korea Foundation for Advance Studies and also a Visiting Professor with the Korea Advance Institute of Science and Technology. He is currently an Associate Professor with the Department of Instrumental & Electrical Engineering, Xiamen University, Xiamen, China. His current research interests include intelligent data analysis, computational intelligent, time-series modeling and applications. He is the author or co-author of several technical papers and also a very active reviewer for many international journals and conferences.

Dr. Zeng is currently serving as an Associate Editor for *Neurocomputing*, and also Editorial Board members for Computers in Biology and Medicine and Biomedical Engineering Online. He also serves as a technical program committee member for ICBEB 2014, an Invited Session Chair of ICCSE 2017.

Zidong Wang (SM'03–F'14) was born in Jiangsu, China, in 1966. He received the B.Sc. degree in mathematics from Suzhou University, Suzhou, China, in 1986, and the M.Sc. degree in applied mathematics and the Ph.D. degree in electrical engineering both from the Nanjing University of Science and Technology, Nanjing, China, 1990 and 1994, respectively.

He is currently a Professor of Dynamical Systems and Computing with the Department of Computer Science, Brunel University London, London, U.K. From 1990 to 2002, he held teaching and research appointments in universities in China, Germany, and the UK. His research interests include dynamical systems, signal processing, bioinformatics, control theory and applications. He has authored more than 600 papers in refereed international journals. He is a holder of the Alexander von Humboldt Research Fellowship of Germany, the JSPS Research Fellowship of Japan, William Mong Visiting Research Fellowship of Hong Kong.

Dr. Wang serves (or has served) as the Editor-in-Chief for Neurocomputing, Deputy Editor-in-Chief for International Journal of Systems Science, and an Associate Editor for 12 international journals including the IEEE TRANSACTIONS ON AUTOMATIC CONTROL, the IEEE TRANSACTIONS ON CONTROL SYSTEMS TECHNOLOGY, the IEEE TRANSACTIONS ON NEURAL NETWORKS, the IEEE TRANSACTIONS ON SIGNAL PROCESSING, and the IEEE TRANSACTIONS ON SYSTEMS, MAN, AND CYBERNETICS-PART C. He is a Fellow of the Royal Statistical Society and a member of program committee for many international conferences.

Hong Zhang received the bachelor's degree in electrical engineering and automation from the Department of Mechanical & Electrical Engineering, Xiamen University, Xiamen, China, in 2015, where she is currently working toward the master's degree from the Department of Electrical Testing Technology and Instruments. Her research interests include image processing and deep learning techniques.

Kee-Eung Kim received the B.S. degree in computer science from KAIST, Daejeon, South Korea, in 1995, and the ScM and Ph.D. degrees in computer science from Brown University, Providence, RI, USA, in 1998 and 2001, respectively. From 2001 to 2006, he was a Senior Software Engineer with Samsung SDS, South Korea, and a Senior Research Staff Member with the Samsung Advanced Institute of Technology, South Korea. In 2006, he joined the Faculty of Computer Science Department with KAIST, where he is currently an Associate Professor. His research interests are representations and algorithms for sequential decision making problems in artificial intelligence and machine learning, including Markov decision processes and reinforcement learning.

Yurong Li was born in Fujian Province, China, in 1973. She received the master's degree in industry automation and the Ph.D. degree in control theory and control engineering from Zhejiang University, Zhejiang, China, in 1997 and 2001, respectively.

She is currently a Professor with Fuzhou University, Fuzhou, China. Especially, she is the Director with Fujian Key Laboratory of Medical Instrumentation & Pharmaceutical Technology, Fuzhou, China. Her research interests include biomedical instrument and intelligent information processing.

Xiaohui Liu received the B.Eng. degree in computing from Hohai University, Nanjing, China, in 1982 and the Ph.D. degree in computer science from Heriot-Watt University, Edinburg, U.K., in 1988.

He is a Professor of Computing with Brunel University London, Uxbridge, U.K., where he directs the Centre for Intelligent Data Analysis. He has more than 100 journal publications in computational intelligence and data science. He was the recipient of the Highly Cited Researchers Award by Thomson Reuters.